Similarity Relationships in the Marine Atmospheric Surface Layer for Terms in the TKE and Scalar Variance Budgets*

J. B. EDSON

Woods Hole Oceanographic Institution, Woods Hole, Massachusetts

C. W. FAIRALL

NOAA/Environmental Technologies Laboratory, Boulder, Colorado

(Manuscript received 3 September 1996, in final form 25 October 1997)

ABSTRACT

Measurements of the momentum, heat, moisture, energy, and scalar variance fluxes are combined with dissipation estimates to investigate the behavior of marine surface layer turbulence. These measurements span a wide range of atmospheric stability conditions and provide estimates of z/L between -8 and 1. Second- and third-order velocity differences are first used to provide an estimate of the Kolmogorov constant equal to 0.53 $\pm$ 0.04. The fluxes and dissipation estimates are then used to provide Monin–Obukhov (MO) similarity relationships of the various terms in the turbulent kinetic energy (TKE) and scalar variance (SV) budgets. These relationships are formulated to have the correct limiting forms in extremely stable and convective conditions. The analyses concludes with a determination of updated dimensionless structure function parameters for use with the inertial–dissipation flux method.

The production of TKE is found to balance its dissipation in convective conditions and to exceed dissipation by up to 17% in near-neutral conditions. This imbalance is investigated using the authors' measurements of the energy flux and results in parameterizations for the energy flux and energy transport term in the TKE budget. The form of the dimensionless energy transport and dimensionless dissipation functions are very similar to previous parameterizations. From these measurements, it is concluded that the magnitude of energy transport (a loss of energy) is larger than the pressure transport (a gain of energy) in slightly unstable conditions.

The dissipation of SV is found to closely balance production in near-neutral conditions. However, the SV budget can only be balanced in convective conditions by inclusion of the transport term. The SV transport term is derived using our estimates of the flux of SV and the derivative approach. The behavior of the derived function represents a slight loss of SV in near-neutral conditions and a gain in very unstable conditions. This finding is consistent with previous investigations.

The similarity between these functions and recent overland results further suggests that experiments are generally above the region where wave-induced fluctuations influence the flow. The authors conclude that MO similarity theory is valid in the marine surface layer as long as it is applied to turbulence statistics taken above the wave boundary layer.

1. Introduction

Our understanding of the behavior of turbulence in the atmospheric surface layer was vastly improved by a number of overland field experiments conducted during the late 1960s and 1970s. These include the landmark 1968 Kansas (Izumi 1971) experiment, the 1973 Minnesota (Champagne et al. 1977) experiment, and the 1976 International Turbulence Comparison Experiment (Dyer and Bradley 1982). These experiments led to the validation of a powerful set of statistical tools derived from Monin–Obukhov similarity theory. The semiempirical relationships derived from their carefully conducted measurements are now used extensively in the lower boundary conditions of numerical forecast models where one must derive turbulent quantities from the mean variables available from the model. Similarly, these relationships are often used to estimate the desired turbulent quantities from mean measurements over the ocean where direct measurement of the fluxes is very difficult. However, the use of overland measurements to infer surface fluxes over the open ocean raises questions about the universality of these relationships.

There have been a number of experiments to investigate the structure of atmospheric turbulence in the marine boundary layer (Smith et al. 1996). These include the 1969 Barbados Oceanographic and Meteorological

* WHOI Contribution Number 9316.

Corresponding author address: Dr. James B. Edson, WHOI MS#10, 98 Water Street, Woods Hole, MA 02543.
E-mail: jedson@whoi.edu

Experiment (Keuttner and Holland 1969) and the 1974 North Pacific Experiment (Schmitt et al. 1979). Both of these experiments were conducted aboard the Floating Instrument Platform (R/P *FLIP*), which allows researchers to make flux measurements over the open ocean from a stable platform. Though these experiment were successful on many fronts, they both suffered from the now well-known (but still difficult to overcome) problem of sea salt contamination of their temperature probes (Schmitt et al. 1978). Large and Pond (1981, 1982) used the Bedford Institute of Oceanography spar buoy plus ship data in a landmark study of fluxes and transfer coefficients over a broad range of wind speeds.

The 1986 Humidity Exchange Over the Sea (HEXOS) (Katsaros et al. 1987) main experiment deployed instrumentation designed to avoid environmental contamination problems. This effort included a number of instruments designed to remove the effects of sea spray (Katsaros et al. 1994), as well as the use of sonic thermometers to compute the temperature fluctuations (Larsen et al. 1993). The HEXOS investigations were conducted from a platform located 10 km off the Dutch coast. The results from this experiment confirmed a number of earlier results, for example, that the production of turbulence kinetic energy (TKE) is closely balanced by its dissipation (Edson et al. 1991) and that the drag coefficient is a function of wave age at a given wind speed (Smith et al. 1992; Maat et al. 1991). The experiment also demonstrated that the transfer coefficients for temperature and humidity were only weakly dependent on wind speed (DeCosmo et al. 1996), although the significance of these results remains a hotly debated topic (e.g., Katsaros and de Leeuw 1994; Andreas 1994; Andreas et al. 1995).

In recent years, a number of researchers have made a great deal of progress in computing direct covariance flux estimates from ocean-going platforms (e.g., Fujitani 1981, 1985; Tsukamoto et al. 1990; Bradley et al. 1991; Fairall et al. 1997; Edson et al. 1998). In the case of moving platforms, this requires systems that are capable of removing platform motion from our velocity measurements before computing the fluxes (Fujitani 1985). This generally involves the integration of linear accelerometers and angular rate sensors to compute the high-frequency motion of the platform that are combined with the low-frequency velocity measurements from global positioning systems and/or current meters (e.g., Edson et al. 1998). Similar measurements from buoy mounted instrumentation can be found in Anctil et al. (1994). For example, direct covariance flux estimates were collected from ship-mounted systems during the Tropical Ocean Global Atmosphere (TOGA) Coupled Ocean–Atmosphere Response Experiment (COARE) in the equatorial Pacific Ocean (Webster and Lukas 1992). These flux estimates have been used to develop a bulk algorithm based on the parameterizations proposed by Liu et al. (1979), Smith (1988), and Godfrey and Beljaars (1991). The hybrid model includes new semiempirical formulas that improve the performance of the code in very convective conditions as reported by Fairall et al. (1996a) and Fairall et al. (1996b).

Despite the emergence of covariance flux measurements from ships, interest remains high in the inertial–dissipation flux estimation method (Large and Pond 1982; Fairall and Larsen 1986). Papers frequently appear in the literature using this method (e.g., Anderson 1993; Yelland and Taylor 1996; Fairall et al. 1996a; Frederickson et al. 1997), which is now being used extensively on buoy-based systems (Skupneiwicz and Davidson 1991; Yelland et al. 1994). It is clear that inertial–dissipation stress data give much lower scatter than covariance estimates (Fairall et al. 1996a) and there is substantial evidence that covariance stresses are much more influenced by flow distortion (Edson et al. 1991; Oost et al. 1994).

Inertial–dissipation measurements still represent the vast majority of data used to determine the drag coefficient over the open ocean at wind speeds greater than 20 m s^{-1}. The disadvantage of this method is that it relies on Monin–Obukhov similarity and requires specification of the dimensionless structure function parameters. These are empirical functions and the method is uncertain to the extent that these functions are uncertain. Forms of these functions determined over Kansas are still being used (Wyngaard and Cote 1971; Wyngaard et al. 1971a,b), but demands for ever-increasing accuracy in flux estimates and bulk transfer coefficients require us to continually refine these functions.

In this paper we present an analysis of data recently taken in the marine surface layer aboard the R/P *FLIP* and the R/V *Columbus Iselin.* These new measurements feature direct eddy correlation stress and heat flux estimates, and TKE and scalar variance (SV) dissipation computed from the inertial subrange of the velocity, temperature, and specific humidity spectra. The high-frequency velocity and temperature measurements were made using sonic anemometers–thermometers, while the specific humidity measurements were made using infrared hygrometers. The data collected during these two experiments cover a much wider stability range than any of the above mentioned datasets. In particular, the extremely unstable data will allow us to examine the behavior of the turbulence statistics in the free convective limit.

The focus of this investigation is the evaluation of the components of the TKE and SV budgets and their relationship to the inertial subrange variables. Our goal is to verify and extend the overland results for application over the oceans including a closer look at the relative balance of turbulent and pressure transport in the TKE budget. In the sections that follow we begin with a brief overview of Monin–Obukhov similarity theory. This is followed by a description of the field programs, the instruments, and the data processing techniques in section 3. Dissipation estimates and evaluation of the Kolmogorov constant using the skewness rela-

tions of Kolmogorov (1941) are discussed in section 4. The TKE budget is evaluated in section 5; the SV budgets in section 6; and the dimensionless structure function parameters are given in section 7.

2. Similarity theory

The structure of the turbulent flow in the surface layer is influenced by both mechanical and thermal forcing. Obukhov (1946) and Monin and Obukhov (1954) were the first to describe a similarity hypothesis about the statistical nature of the turbulent flow based on the relative strength of these two forcing mechanisms. Monin–Obukhov (hereafter MO) similarity theory states that the structure of turbulence is determined by the height above the surface z, the buoyancy parameter $g/\overline{\Theta}_v$, the friction velocity u_*, and the surface buoyancy flux $\overline{w\theta}_{v0}$, where $\overline{\Theta}_v$ is the virtual potential temperature and g is the acceleration of gravity (e.g., Wyngaard 1973). These last two terms are defined from the surface stress and heat fluxes as

$$u_* = \left[\frac{|\boldsymbol{\tau}_0|}{\rho}\right]^{1/2}, \tag{1}$$

$$\overline{w\theta}_{v_0} = \frac{Q_0}{\rho c_p} + 0.61T_0\frac{E_0}{\rho L_e}, \tag{2}$$

where $\boldsymbol{\tau}_0$ is the surface stress vector (the surface value of the momentum flux), Q_0 is the surface value of the sensible heat flux, E_0 is the surface value of the latent heat flux, ρ is the density of air, c_p is the specific heat at constant pressure, and L_e is the latent heat of vaporization of water.

One of the basic assumptions of MO similarity theory is that these fluxes are constant with height in the surface layer. In reality, this constant flux assumption is never truly valid in the atmospheric boundary layer. However, a good approximation to this constant flux assumption is obtained if we define the top of the surface layer as that height where the momentum flux is 90% of its surface value. Since the momentum flux generally decreases linearly with height, this definition results in a surface layer that occupies the lowest 10% of the atmospheric boundary layer.

The unstable marine boundary layers studied in this paper were typically 500–700 m in height, which results in a surface layer height of approximately 60 m. This allows us to estimate the surface fluxes from our covariance measurements (made at about 12 m height) as

$$\frac{\boldsymbol{\tau}_0}{\rho} \approx \frac{\boldsymbol{\tau}}{\rho} = -\mathbf{i}\overline{uw} - \mathbf{j}\overline{vw}, \tag{3}$$

$$Q_0 \approx Q = \rho c_p\overline{w\theta}, \tag{4}$$

$$E_0 \approx E = \rho L_e\overline{wq}, \tag{5}$$

where u, v, and w are longitudinal, lateral, and vertical velocity fluctuations, respectively; θ are temperature fluctuations; and q are specific humidity fluctuations.

a. The marine surface layer

In addition to the constant flux layer constraint, the application of MO similarity theory to the marine surface layer requires some caution because the scaling parameters are only meant to account for the influence of mechanical and thermal forcing on the turbulence. Many investigations such as those by Geernaert et al. (1986), Rieder et al. (1994), Donelan et al. (1993), and Hare et al. (1997) have demonstrated that additional scaling parameters are required to describe turbulent variables within the wave boundary layer (WBL). The WBL is defined in this paper as the layer where the total momentum flux, even if assumed to be constant with height, has appreciable turbulent and wave-induced components. That is, within the WBL the momentum equation can be written as

$$\frac{\partial}{\partial z}\left(-\overline{\tilde{u}\tilde{w}} - \overline{u'w'} + \nu\frac{\partial\overline{U}}{\partial z}\right) \approx 0, \tag{6}$$

where primes denote turbulent fluctuations, tildes denote the wave-induced fluctuations, $\overline{U}$ is the mean wind [i.e., $U(t) = \overline{U} + u'(t) + \tilde{u}(t) = \overline{U} + u(t)$], and the last term on the right-hand side represents the viscous stress where ν is the kinematic viscosity.

To examine the applicability of MO similarity theory in the marine surface layer, we are limiting our analyses to observations where the flow is not expected to be influenced by wave-induced fluctuations. We believe that we are meeting this constraint based on the fact that the measurement heights for the R/P *FLIP* (12 m) and R/V *Iselin* (11.5 m) are generally larger than the reciprocal wavenumber of the dominant wind waves, k_w^{-1}, observed during our respective cruises (i.e., in general, $k_w z > 1$). Therefore, although we have reason to believe that we are experiencing wave-induced effects at our highest winds (see section 8), we believe that most of our dataset is characteristic of a surface layer where the turbulent fluxes dominate the total flux and MO similarity theory is applicable.

b. Monin–Obukhov scaling

Monin–Obukhov similarity theory is covered in detail in a number of texts, including Lumley and Panofsky (1963) and Wyngaard (1973). For the purposes of this paper we briefly describe the basis MO similarity theory by first combining the four governing parameters to form an additional velocity scale defined as

$$u_f = \left(\frac{zg}{\overline{\Theta}_v}\overline{w\theta}_{v_0}\right)^{1/3}, \tag{7}$$

whose use is restricted to positive values of the heat flux (i.e., convective conditions). The two velocity

scales, u_* and u_f, are then used to define two temperature and moisture scales,

$$T_* = -\frac{\overline{w\theta}_0}{u_*}, \qquad T_f = -\frac{\overline{w\theta}_0}{u_f}, \tag{8}$$

$$q_* = -\frac{\overline{wq}_0}{u_*}, \qquad q_f = -\frac{\overline{wq}_0}{u_f}, \tag{9}$$

and a length scale now known as the Monin–Obukhov length,

$$L = -\frac{\overline{\theta}_v}{g\kappa}\frac{u_*^3}{\overline{w\theta}_0}, \tag{10}$$

where κ is the von Kármán constant. The magnitude of the MO length is determined by the relative strength of the mechanical versus thermal forcing, while its sign is determined by the sign of the buoyancy flux; that is, it is negative in convective (unstable) conditions and positive in stratified (stable) conditions.

The various scales are not independent (Wyngaard 1973) as they can be combined to obtain

$$\frac{u_f}{u_*} = \left(-\frac{z}{\kappa L}\right)^{1/3} \tag{11}$$

and

$$\frac{T_f}{T_*} = \frac{q_f}{q_*} = \left(-\frac{z}{\kappa L}\right)^{-1/3} \tag{12}$$

in convective conditions. Therefore, it is common practice to select u_*, T_*, and q_* as the velocity, temperature, and moisture scales for both stable and unstable flows. The similarity hypothesis then states that various turbulent statistics, when normalized by these scaling parameters, are a universal function of z/L. This hypothesis has been validated by a number of studies in the atmospheric boundary layer over land. Notable examples include the studies by Dyer and Hicks (1970), Wyngaard and Coté (1971), Kaimal et al. (1972), Champagne et al. (1977), and Dyer and Bradley (1982).

In light winds conditions with appreciable heat flux, MO similarity theory requires that the surface stress (i.e., u_*) is no longer a relevant scaling parameter and that the small-scale turbulence variables approach the convective limits. In this limit the structure of the marine atmospheric surface layer in the region between $-L < z < 0.1\, z_i$ should approach that of local free convection and depend only on z, $g/\overline{\Theta}_v$, and $\overline{w\theta}_{v0}$ (Tennekes 1970). Under these conditions it is more appropriate to use the convective scaling parameters denoted by the subscript f. Additionally, above the surface layer (i.e., $z > 0.1\, z_i$), studies of the mixed layer have shown that many turbulent processes scale with the height of the boundary layer, z_i. In this region, z_i replaces z as the appropriate length scale and one uses the free-convective velocity scale proposed by Deardorff (1970):

$$w_* = \left(\frac{z_i g}{\overline{\Theta}_v}\overline{w\theta}_{v_0}\right)^{1/3}. \tag{13}$$

Overland studies involving this type are scaling analysis have been reported by Wyngaard et al. (1978), Wyngaard and LeMone (1980), and Højstrup (1982).

3. Field programs and data processing

In this paper we present analyses of data taken in two recent experiments in the marine surface layer aboard the R/P *FLIP* and the R/V *Columbus Iselin.* These two experiments used similar instruments, data acquisition systems, and processing techniques to estimate the turbulent statistics. One experiment was an open ocean location just outside the islands off Los Angeles, California; the other was in the vicinity of the Gulf Stream edge off Cape Hatteras. Details about the instruments and basic processing are provided in this section. The overall quality of the covariance fluxes is illustrated by comparison with bulk flux estimates.

The R/P *FLIP* was deployed off the west coast of southern California for a 2-week period during the second half of September 1993 as part of the San Clemente Ocean Probing Experiment described in Kropfli and Clifford (1994). The R/P *FLIP* was positioned off San Clemente Island, California (33°N, 118°W). Data were obtained in the wind-speed range from 0.5 to 12 m s^{-1}, with sea–air temperature differences from 0° to 4°C. The Environmental Technologies Laboratory's ship flux measurement system was used. This system is described in detail by Fairall et al. (1997), so only a brief sketch will be given here.

A sonic anemometer–thermometer is used to make measurements of the stress and buoyancy flux, and a fast-response infrared hygrometer is used with the sonic anemometer to obtain the latent heat flux. A dual inertial navigation system is used to correct for ship motions (Edson et al. 1998). Fluxes were computed using covariance, inertial–dissipation, and bulk techniques. Sea surface temperature is derived from bulk water measurements at a depth of 5 cm with a floating thermistor and the corrections for the cool skin effect described in Fairall et al. (1996b). Mean air temperature and humidity are derived from a conventional aspirated T/RH sensor; the infrared hygrometer provided redundant information. The instruments were deployed at the end of *FLIP*'s 20-m-long port boom. Editing for radio interference and fog contamination yielded 180 usable 50-min averages.

The second dataset was taken aboard the R/V *Columbus Iselin* in June 1993 as part of the Office of Naval Research's (ONR) High Resolution Program. The experiment was designed to investigate the cause of the surface features seen in remotely sensed images of the sea surface around the northern edge of the Gulf Stream. Sea surface temperatures in this region ranged between 22° and 29°C and often resulted in a change in the sign

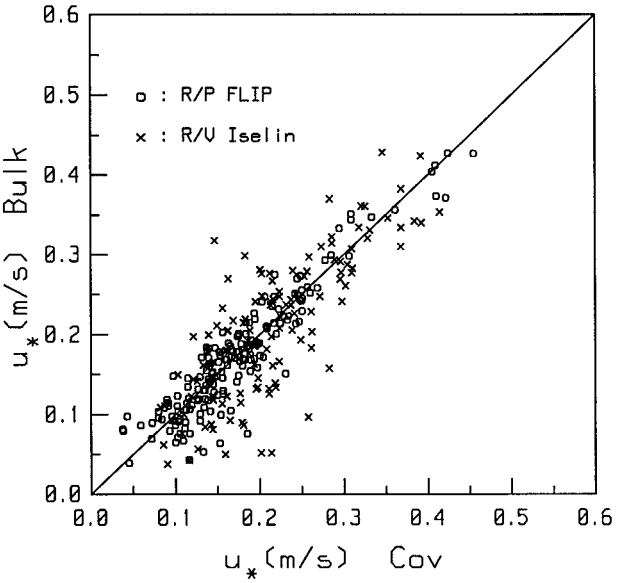

FIG. 1. A comparison of the friction velocities, u_*, estimated using the bulk aerodynamic vs direct covariance methods. The friction velocity estimates for the R/P *FLIP* are computed from 50-min averages, while the R/V *Iselin* estimates are taken from 30-min averages.

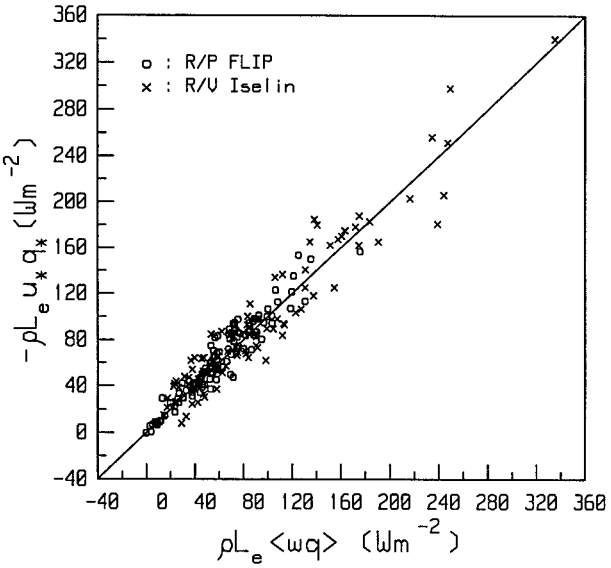

FIG. 2. A comparison of the latent heat fluxes estimated using the bulk aerodynamic vs direct covariance methods. The averaging times are as in Fig. 1.

of the stability as the ship crossed the Gulf Stream edge. The advection of warm air over cooler water during a portion of the experiment resulted in a number of measurements made under stable conditions. As a result, the combined datasets cover a stability range $-8 < z/L < 1$, which allows us to investigate the scaling laws in the limits of both local free convection and extremely stable stratification.

Our estimates of the surface stress, and therefore u_*, are computed using the eddy correlation technique. Our estimates of the dissipation rate of TKE are determined from the sonic velocity spectra as described in the following section. Our estimates of the dissipation rate of temperature and humidity variance are computed from the sonic temperature and infrared hygrometer humidity spectra, respectively. The Monin–Obukhov lengths were determined using the buoyancy flux from the sonic anemometer and a von Kármán constant of 0.4.

The R/P *FLIP* and the R/V *Iselin* data were corrected for contamination due to platform motion using strapdown accelerometers and rate sensors as described in Edson et al. (1998). The corrections on *FLIP* were much smaller than on the *Iselin,* resulting in somewhat more uncertainty in the *Iselin* measurements. Additionally, the *Iselin* data exhibit more scatter near neutral stratification because these conditions are usually the result of being near the Gulf Stream edge where conditions are inhomogeneous. In fact, we have found that the removal of a few data points where the sign of the heat flux does not match the sign of the sea–air temperature greatly reduces the scatter in our comparisons. Therefore, we have taken this approach in the following analysis to remove data collected during very inhomogeneous conditions.

We compare our direct covariance estimates of the scaling parameters with bulk estimates calculated using the TOGA COARE algorithm (Fairall et al. 1996a) in Figs. 1–3. The present data are comparable to the COARE results, with *FLIP* data being significantly better for u_*, where motion corrections and flow distortion play a smaller role than in the ship-based measurements. Thus, the greater scatter in the *Iselin* estimates is most obvious in the u_* comparison given in Fig. 1. In this figure, the *Iselin* momentum flux estimates have been reduced by 15% (a 7% reduction in u_*) based on the R/P *FLIP* versus ship comparison presented in Edson et al. (1998), which accounts for the effect of flow distortion by the ship's superstructure. Once we have applied this correction we obtain very good agreement between the direct covariance and bulk momentum and heat flux estimates over a wide range of conditions. This is particularly true of the latent heat flux estimates shown in Fig. 2, which has been a difficult variable to measure directly (or even indirectly) over the open ocean.

4. Inertial–dissipation and third-order structure function estimates

a. Inertial–dissipation estimates

The dissipation rate of turbulent kinetic energy is one of the most widely used variables in investigations of both atmospheric and oceanic boundary layers. Direct measurements of the dissipation rate are usually accomplished by taking the spatial or time derivative of hot-wire anemometers signals. The use of hot wires is necessary because the anemometers must be fast enough to measure fluctuations with a spatial resolution that

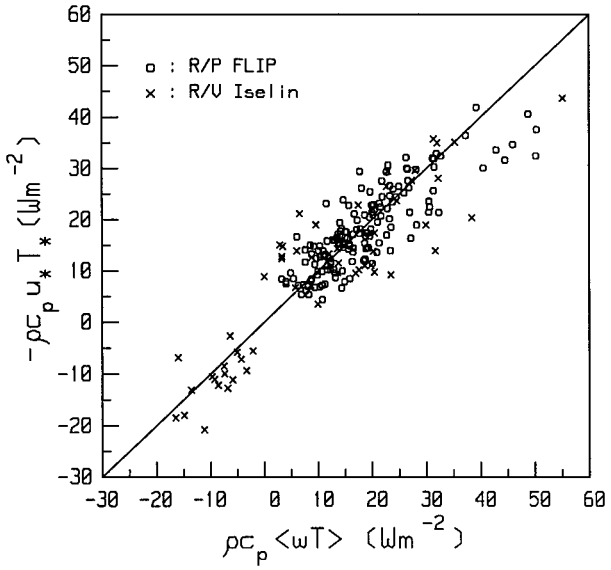

FIG. 3. A comparison of the sensible heat fluxes estimated using the bulk aerodynamic vs direct covariance methods. The averaging times are as in Fig. 1.

approaches the Kolmogorov microscale, $\eta = (\nu^3/\epsilon)^{1/4}$, which is typically 1 mm in atmospheric flows.

Unfortunately, the use of hot-wire anemometry over the ocean is severely limited by the contamination and frequent destruction of the wires by sea spray. As a result, dissipation rates in the atmospheric marine surface layer are usually computed from one-dimensional variance spectra measured with sonic anemometers. In the inertial subrange of isotropic turbulence, the one-dimensional velocity variance spectrum Φ_u can be expressed as a function of wavenumber magnitude,

$$\Phi_u(k) = \alpha_u \epsilon^{2/3} k^{-5/3}, \tag{14}$$

where ϵ is the dissipation of TKE into heat, k is the wavenumber, and α_u is the one-dimensional Kolmogorov constant. These spectra can be related to the frequency spectra S_u, commonly measured in the field using Taylor's hypothesis (here, $k = 2\pi f/\overline{U}$) as

$$k\Phi_u(k) = \frac{fS_u(f)}{T_{uu}} = \alpha_u \epsilon^{2/3} \left(\frac{2\pi f}{\overline{U}}\right)^{-2/3}, \tag{15}$$

where T_{uu} is a factor that corrects for inaccuracies in using Taylor's hypothesis to estimate the magnitude of wavenumber spectra in the inertial subrange. We use the form given by Wyngaard and Clifford (1977),

$$T_{uu} = 1 - \frac{1}{9}\frac{\sigma_u^2}{(\overline{U})^2} + \frac{2}{3}\frac{(\sigma_v^2 + \sigma_w^2)}{(\overline{U})^2}, \tag{16}$$

where the standard deviations are computed from the same time series that produced the spectral estimate (Hill 1996). This correction reduces our spectral estimates by an average of 2%. Therefore, (15) can be used to find estimates of the dissipation rates from our longitudinal velocity spectra if we know the value of the Kolmogorov constant. Estimate of this constant have been determined from direct measurement of ϵ using hot-wire anemometry in several overland experiments. A review of these measurements by Högström (1996) suggested a value of 0.52.

b. *Third-order structure function dissipation estimates*

Another method that can be use to measure ϵ and determine the Kolmogorov constants relies on the skewness coefficient for the distribution of velocity differences as described by Kolmogorov (1941). The skewness

$$S = \frac{B_{uuu}(r)}{[B_{uu}(r)]^{3/2}} \tag{17}$$

is computed using the ratio of the second- and third-order velocity differences,

$$B_{uu}(r) = \overline{[U(x) - U(x + r)]^2}, \tag{18}$$

$$B_{uuu}(r) = \overline{[U(x) - U(x + r)]^3}, \tag{19}$$

where $U(x)$ and $U(x + r)$ are instantaneous longitudinal velocity measurements separated by a distance, r, in the direction of the longitudinal wind. In the inertial subrange these parameters are related to the structure function parameter C_u^2 and the dissipation rates by

$$\frac{B_{uu}(r)}{r^{2/3}} = C_u^2 = 4.0\alpha_u \epsilon^{2/3} \tag{20}$$

and

$$\frac{B_{uuu}(r)}{r} = -\frac{4}{5}\epsilon. \tag{21}$$

Based on these expressions, Kolmogorov (1941) hypothesized that in the inertial subrange the skewness should remain constant. Using this hypothesis and the above equations, Kolmogorov obtained an expression that can be used to compute the one-dimensional Kolmogorov constant as

$$\alpha_u = \left(-\frac{1}{10S}\right)^{2/3}. \tag{22}$$

The skewness of the longitudinal velocity fluctuations has been reported by a number of researchers (e.g., see the review by van Atta and Chen 1970). In general, these researchers have relied on hot-wire anemometry to compute these statistics. A notable exception involves the work of Paquin and Pond (1971), who produced estimates of the Kolmogorov constants using sonic anemometer measurements by invoking Taylor's hypothesis; for example, $r = \overline{U}\Delta t$.

Paquin and Pond (1971) describe in some detail the constraints that restrict the choice of the appropriate

spatial separations for determination of the Kolmogorov constants. The two constraints required of all such measurements are that r be much smaller than the scale of the energy-containing eddies and much larger than the Kolmogorov microscale in order to be in the inertial subrange. The first constraint is generally met if we confine our measurements to separation distances that are smaller than our measurement heights, that is, $r/z < 1$. The second constraint is never an issue because $r \gg \eta$, even at our lowest recorded wind speed.

Additionally, the use of a sonic anemometer requires r to be much larger than the size of the instrument. This constraint, which arises because of the spatial averaging associated with sonic anemometers (Kaimal et al. 1968; Larsen et al. 1993), requires us to limit our analysis to separation distances much larger than the distance between the sonic transducers, L. While the effect of spatial averaging on $B_{uuu}(r)$ is negligible in the inertial subrange (Stewart 1963; Hill 1996), its effect on $B_{uu}(r)$ can be substantial. Stewart (1963) and Hill (1996) have derived expressions to account for the effect of spatial averaging on second-order statistics. They have shown that for $r/L \gg 1$,

$$B_{uu}(r) = C_u^2 r^{2/3}\left[1 - \frac{1}{54}\left(\frac{L}{r}\right)^2 - \frac{9}{20}\left(\frac{L}{r}\right)^{2/3}\right] = C_u^2 r^{2/3} V_{uu}\left(\frac{L}{r}\right), \quad (23)$$

such that the structure function requires an additional correction,

$$C_u^2 = \frac{\overline{[U(t) - U(t + \Delta t)]^2}}{(\overline{U}\,\Delta t)^{2/3} T_{uu} V_{uu}(L/r)}. \quad (24)$$

We note that $\Phi_u(k)$ forms a transform pair with $B_{uu}(r)$ (Tatarskii 1971), which results in the relationship given by (20). However, this also means that $\Phi_u(k)$ requires correction for spatial averaging. This correction is obtained from the Fourier transform of (23) given by

$$\Phi_u(k) = \frac{1}{\pi}\Gamma\left(\frac{5}{3}\right)\sin\left(\frac{\pi}{3}\right)C_u^2 k^{-5/3} - \frac{L^2}{54\pi}\Gamma\left(-\frac{1}{3}\right) \times \sin\left(-\frac{2\pi}{3}\right)C_u^2 k^{1/3} \approx 0.25 C_u^2 k^{-5/3}[1 - 0.083(kL)^2], \quad (25)$$

where the first term is responsible for the constant in (20). The correction term hardly affects our inertial subrange estimates of ϵ over the wavenumber range used in our analyses, namely, $kL < 1$.

Finally, interpretation of our measurements is simplified if we confine our investigations to look at the correlation between signals with zero lags, that is, to variances and covariances that are computed from correlations between variables measured at the same instant in time. The second constraint avoids the complications that arise from spatial displacements caused by the platform that cannot be handled by Taylor's hypothesis (e.g., Lumley and Terray 1983). Nonetheless, it appears that the *FLIP* data are usable to examine the lagged quantities much better than the shipboard measurements owing to its small horizontal and vertical displacements. Therefore, we confine our investigation of the skewness to the *FLIP* dataset.

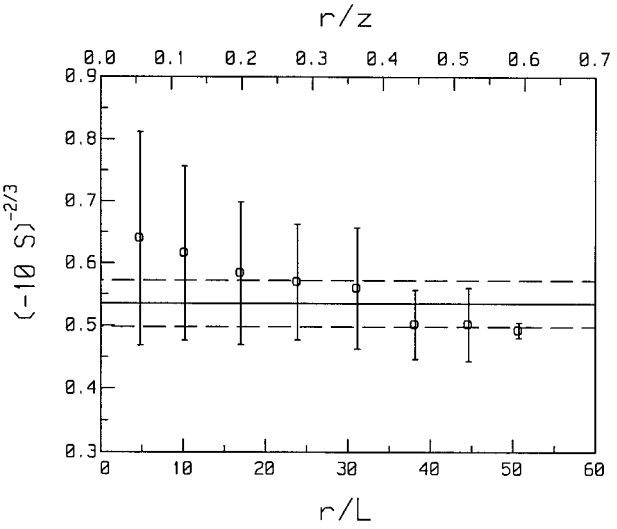

FIG. 4. Estimates of the Kolmogorov constant computed using (22) as a function of the dimensionless length r/z. The lines in the figure denotes a value of 0.53 (solid lines) ± 0.04 (broken lines).

The average of all of the individual *FLIP* measurements of (22) that met the constraints $r/L > 10$ and $r/z < 1$ gives a Kolmogorov constant of 0.57 ± 0.10. Additionally, if we first compute the average skewness using these same constraints and then use the average skewness in (22), we obtain a value of 0.55. These values are in remarkably good agreement with those determined by Paquin and Pond (1971), who derived a value of 0.57 ± 0.10 using individual estimates of (22) and a value of 0.54 using the average skewness.

The dependence of our estimates of the Kolmogorov constant on the constraints given above can be examined by averaging estimates of (22) in bins of r/L. These bin-averaged estimates are shown in Fig. 4 along with the equivalent values of r/z. It is interesting to note that these estimates span the range of estimates reported in the literature and approach a value of 0.50 at large values of r/L. This suggests that the various constraints considered above are responsible for much of the experimental uncertainty. We feel that we can reduce some of the uncertainty in our estimate by using the bin-averaged results. This approach gives more even weight to our estimates over the entire range of r/L. The mean of bin-averaged data between $r/L > 10$ and $r/z < 1$ gives a Kolmogorov constant of 0.53 ± 0.04. Therefore, we use

0.53 in the analysis that follows and recognize that the difference between this value and 0.57 (or 0.49) introduces an uncertainty of approximately 10% in our estimates of the dissipation rate.

5. The TKE budget

The TKE budget equation for stationary and horizontally homogeneous conditions in the surface layer above the wave boundary layer is

$$-\overline{uw}\frac{\partial \overline{U}}{\partial z} - \overline{vw}\frac{\partial \overline{V}}{\partial z} + \frac{g}{\overline{\Theta}_v}\overline{w\theta_v} - \frac{1}{\rho}\frac{\partial \overline{wp}}{\partial z} - \frac{\partial \overline{we}}{\partial z} - \epsilon = 0, \tag{26}$$

where p denotes pressure fluctuations and e is the turbulent kinetic energy defined as $e = 0.5\,[u^2 + v^2 + w^2]$. The first two terms on the left-hand side of (26) represent the generation of mechanical turbulence through shear, while the third term represents the production (suppression) of turbulence through convection (stratification). The final two terms neither produce nor consume TKE; instead they act to redistribute TKE within the atmospheric boundary layer through pressure and energy transport.

According to MO similarity theory, the various terms in the TKE budget are expected to be universal functions of z/L after normalization by the appropriate scaling parameters, kz/u_*^3,

$$\frac{\epsilon \kappa z}{u_*^3} = \phi_\epsilon(\zeta) = \phi_m(\zeta) - \zeta - \phi_{tp}(\zeta) - \phi_{te}(\zeta), \tag{27}$$

where $\zeta = z/L$, ϕ_ϵ is the dimensionless dissipation function, ϕ_{tp} and ϕ_{te} are the dimensionless transport terms, and the dimensionless shear is defined as

$$\phi_m(\zeta) = \frac{\kappa z}{u_*}\left[\left(\frac{\partial \overline{U}}{\partial z}\right)^2 + \left(\frac{\partial \overline{V}}{\partial z}\right)^2\right]^{1/2}. \tag{28}$$

Equation (28) is consistent with our definition of u_* and the following parameterizations for the momentum flux components:

$$-\overline{uw} = \frac{u_* \kappa z}{\phi_m(\zeta)}\frac{\partial \overline{U}}{\partial z} \tag{29}$$

and

$$-\overline{vw} = \frac{u_* \kappa z}{\phi_m(\zeta)}\frac{\partial \overline{V}}{\partial z}. \tag{30}$$

These parameterizations are common applications of MO similarity theory in first-order closure models. They offer a good example of why we are limiting our analysis to heights above the WBL, since we would not expect these expressions to be valid in a region where the waves, in addition to the stability, can effect the velocity field and thereby modify the wind profiles.

In the sections that follow we determine the form of the dimensionless functions in (27) using our combined datasets. The wide range of stabilities present in this dataset allows us to examine the limiting forms of these functions in both the convective and stable limits. The behavior of the various terms in the TKE budget in these limits are predicted using the approach outlined by Wyngaard (1973).

a. Dimensionless dissipation function

The function that describes the stability dependence of the dimensionless rate of dissipation is a key ingredient in the inertial–dissipation method of estimating air–sea fluxes (Fairall and Larsen 1986). A number of observation studies conducted over the sea (e.g., Large and Pond 1981; Edson et al. 1991) have found that the dissipation of TKE is very nearly in balance with its production, which reduces (27) to

$$\phi_\epsilon(\zeta) \approx \phi_m(\zeta) - \zeta. \tag{31}$$

It is easy to show that this form of the dimensionless dissipation function is consistent with its predicted form in local free convection. In this limit we expect the dissipation rate to be proportional to u_f^3/z. This prediction can be combined with (11) to find its form in the local free-convective limit as

$$\phi_\epsilon(\zeta) = \frac{\epsilon \kappa z}{u_*^3} = \frac{\epsilon \kappa z}{u_f^3}\frac{u_f^3}{u_*^3} = -a\zeta, \qquad \zeta < -1, \tag{32}$$

where a is a constant of proportionality. Since shear production and therefore ϕ_m become negligible in this limit, (31) and (32) are identical if the constant of proportionality is equal to one, which is the expected result if production truly equals dissipation. The value of this constant can be determined from our measurements by setting $\phi_m(\zeta) - \phi_{te}(\zeta) - \phi_{tp}(\zeta) = 0$ in (27), which results in

$$a = \epsilon\left(\frac{g}{\overline{\Theta}_v}\overline{w\theta_v}\right)^{-1}. \tag{33}$$

The average value of this constant from all estimates of a found for $-\zeta > 1.5$ is 0.99 ± 0.28. Although the scatter is fairly large, this implies that production balances dissipation in the local free-convective limit.

We now compare this result with our measurements of $\phi_\epsilon(\zeta)$ in Fig. 5. In this figure, the solid line is drawn using (31), and the broken line is drawn using $a = 1$ in (32). Since we are not able to compute an estimate of the dimensionless shear with the present dataset, we have opted for consistency and used a function that has the correct form in the convective limit,

$$\phi_m(\zeta) = (1 - 15\zeta)^{-1/3}, \qquad \zeta < 0, \tag{34}$$

as given by Carl et al. (1973) and more recently by Frenzen and Vogel (1992). This function agrees very well with the commonly used Businger–Dyer formulation in forced convection.

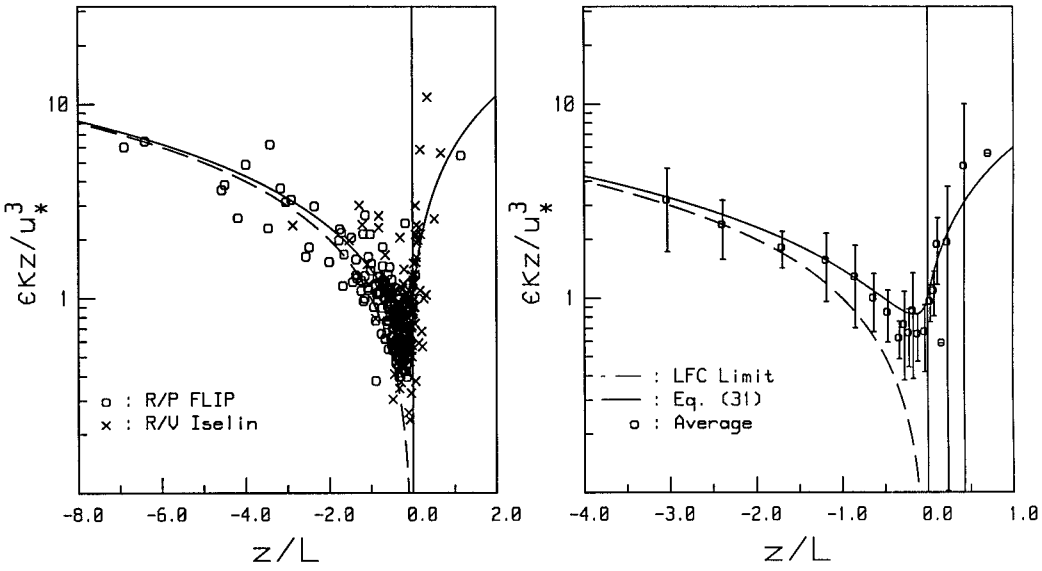

FIG. 5. Estimates of the dimensionless dissipation rate of TKE as a function of z/L. The left-hand panel displays the raw data, while the right-hand panel shows the bin-averaged results. The error bars denote the standard error (standard deviation divided by the number of points). The lines drawn in the figure are identified by the equation numbers as given in the text.

As one would expect, the measurements are in excellent agreement with (31) in very unstable conditions since $a \approx 1$. However, it is clear that this simple parameterization is not accurate for slightly unstable and near-neutral conditions where our data indicate that production exceeds dissipation. This finding is consistent with recent measurements reported by Thiermann and Grassl (1992), Vogel and Frenzen (1992), and Frenzen and Vogel (1992), who also found that production exceeds dissipation in the slightly unstable regime. Their dimensionless dissipation functions are shown in Fig. 6.

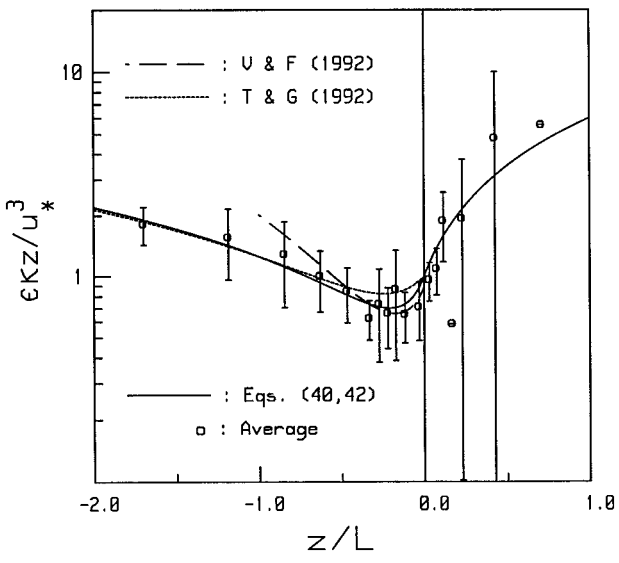

FIG. 6. Functional forms of the dimensionless dissipation functions that include two recently published parameterizations as well as our own functions. The symbols denote bin-averaged results shown in Fig. 5. The solid line drawn in the figure are identified by the equation numbers as given in the text.

The average value of $\phi_\epsilon(\zeta)$ for this dataset is equal to 0.70 over the stability range $-0.1 < \zeta < 0$. This value is in good agreement with the results reported by Garratt (1972), who obtained an average value of $\overline{\phi}_\epsilon = 0.78$ for measurements within the range $-0.1 < \zeta < 0$ using a Kolmogorov constant of 0.50. This value would be reduced to 0.71 using a Kolmogorov constant of 0.53. This slightly unstable estimate is also in agreement with the neutral values of dimensionless dissipation, $\phi_\epsilon(0)$, given by Frenzen and Vogel (1992) and Vogel and Frenzen (1992) in two separate experiments. Their neutral values ranged from 0.84 to 0.89.

b. Dimensionless transport terms

The balance between production and dissipation in free-convective conditions implies that we are using the correct value for the Kolmogorov constant. This assumption further implies that the imbalance at near-neutral conditions is due to the exclusion of the transport terms in our simple parameterization. The direct determination of the energy transport terms in (26) requires flux estimates at multiple levels that are not available in our datasets. However, we can use the wide range of stability in our datasets to our advantage by estimating these terms using the derivative method described in Wyngaard and Coté (1971) and Wilczak et al. (1995). In this method the normalized fluxes are plotted as a

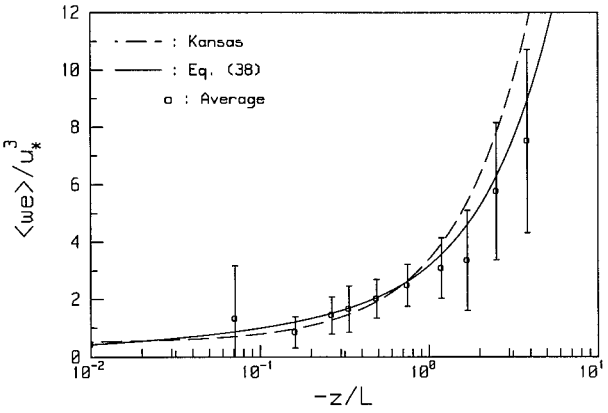

FIG. 7. Estimates of the dimensionless energy flux as a function of z/L. The symbols represent our bin-averaged results. The error bars denote the standard error. The lines drawn in the figure are identified by the equation numbers as given in the text.

function of ζ to determine the dimensionless energy flux function,

$$\phi_e(\zeta) = \frac{\overline{we}}{u_*^3}. \tag{35}$$

This flux should scale with u_f^3 in the convective limit, which leads to the prediction

$$\frac{\overline{we}}{u_*^3} = \frac{\overline{we}}{u_f^3}\frac{u_f^3}{u_*^3} = -\frac{c}{\kappa}, \qquad \zeta < -1, \tag{36}$$

where c is another numerical constant. The derivative of this function is then combined with the definition of the dimensionless energy transport to obtain a prediction for local free convection,

$$\phi_{te}(\zeta) = \frac{\kappa z}{u_*^3}\frac{\partial \overline{we}}{\partial z} = \kappa\zeta\frac{\partial}{\partial\zeta}\left(\frac{\overline{we}}{u_*^3}\right) = -c\zeta, \qquad \zeta < -1, \tag{37}$$

where we see that the constant is only modified by removal of the von Kármán constant.

The dimensionless energy fluxes are plotted in Fig. 7. The broken line in this figure is drawn using the Kansas results reported by Wyngaard and Coté (1971). Wyngaard and Coté (1971) obtained a value of $c \approx 1.0$ using a von Kármán constant of 0.35 such that $c/\kappa \approx 2.9$. Note that we have added an offset of 0.5 to this line [i.e., (37) becomes $-2.9\zeta + 0.5$] and that our definition of the kinetic energy is related to Wyngaard and Coté's as $q = 2e$. Our near-neutral to moderately unstable results are also in good agreement with the data reported by Garratt (1972), Banke and Smith (1973), and Vogel and Frenzen (1992) over a similar stability range.

To include the behavior of this flux over the entire range of unstable conditions we introduce the function given by

$$\phi_e(\zeta) = 2(-\zeta)^{1/3}(1 - \zeta)^{2/3}, \qquad \zeta < 0, \tag{38}$$

as shown by the solid line in Fig. 7. It provides a good fit to the rapid rise exhibited by the data in near-neutral conditions, as well as the tendency toward a smaller slope as $-\zeta$ increases while retaining the correct local free-convective limit. This function is easily differentiated to obtain the dimensionless energy transport function in unstable conditions as

$$\phi_{te}(\zeta) = \frac{\kappa}{3}[4(-\zeta)^{4/3}(1 - \zeta)^{-1/3} + \phi_e(\zeta)], \qquad \zeta < 0. \tag{39}$$

The results from this study and previous investigations show that the turbulent transport of TKE is a nonnegligible term in the budget equation. Therefore, the observed near-balance between production and dissipation in the free-convective limit suggests that the pressure transport term must be nearly equal in magnitude but opposite in sign to the energy transport. This is in agreement with the findings of McBean and Elliot (1975). Under slightly unstable conditions our results indicate that production significantly exceeds dissipation. This suggests that the magnitude of the TKE transport term (a loss of TKE) is greater than the magnitude of the pressure transport term (a gain of TKE).

Although we believe that the observed deficit is a result of a local imbalance in the transport terms, we recognize that the actual mechanisms responsible for the imbalance are debatable. A recent investigation by Edson et al. (1997) using measurements from the 1995 marine boundary layer (MBL) experiment aboard the R/P *FLIP* indicate that this dissipation deficit is a strong function of sea state, implying that MO similarity theory is not valid even well above the surface under high-wind conditions (see section 8). However, although there is some evidence for this effect under the highest wind conditions, the agreement between our data and recent overland results suggests that the measurements are generally above the WBL. Therefore, we believe that we are in a region of the marine surface layer where MO similarity is a valid hypothesis. As such, we recommend the following dimensionless dissipation function for use in ship-based inertial–dissipation systems:

$$\phi_\epsilon(\zeta) = \frac{(1 - \zeta)}{(1 - 7\zeta)} - \zeta, \qquad \zeta < 0. \tag{40}$$

This function represents a slightly modified form of the function given by Thiermann and Grassl (1992), which retains their function's simplicity while providing better agreement with our data, as shown in Fig. 6.

c. Stable regime

As we move away from neutral conditions into the stable regime, the buoyancy force begins to restrict the

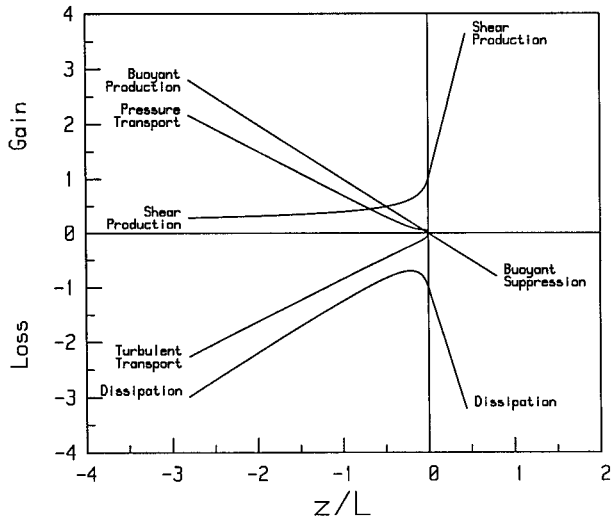

FIG. 8. The dimensionless TKE budget terms proposed in this paper. The buoyant production terms is simply z/L, the shear production is given by (34) and (41); the turbulent transport by (39); and the dissipation by (40) and (42). The pressure transport is the residual of these functions.

production TKE through shear by limiting the size of the energy-containing eddies (i.e., their velocity fluctuations). This is a result of the restoring forces that limits the displacement of the parcels from their equilibrium position. In extremely stable conditions, the size of the eddies are completely limited by the stability (Wyngaard 1973) and they become ''unaware'' of their distance from the surface. The scaling becomes height-independent under these conditions and the MO length becomes the only length scale. As a result, we often refer to such conditions as z-less stratification. This also means that u_* is the only velocity scale because we cannot form another from the three remaining governing parameters.

Under these conditions the variance terms in the TKE budget should go asymptotically as ζ (Wyngaard 1973). Our dimensionless energy flux analysis and the Kansas results indicate that the transport terms are truly negligible in stable conditions such that (31) is an appropriate form of the dimensionless dissipation function. Additionally, the limiting form of the dimensionless shear in very stable conditions suggest that it should go as

$$\phi_m(\zeta) = 1 + e\zeta, \qquad \zeta > 0. \tag{41}$$

This results in a form of the dimensionless dissipation function given by

$$\Phi_\epsilon(\zeta) = 1 + (e - 1)\zeta, \qquad \zeta > 0, \tag{42}$$

where a value of $e = 6$ gives good agreement between our data, as shown in Fig. 6. The form of all of the proposed functions in the TKE budget equation is summarized in Fig. 8, where the pressure transport is derived by subtracting (39), (40), and ζ from (34). These functions are in good agreement with the consensus functions presented by Wyngaard (1992).

6. The scalar variance budgets

The scalar equivalents of the TKE budget equation are the potential temperature and specific humidity variance budgets. In homogeneous and steady-state conditions, these budgets are as follows:

$$\overline{w\theta}\frac{\partial\overline{\Theta}}{\partial z} - \frac{1}{2}\frac{\partial\overline{w\theta^2}}{\partial z} - N_\theta = 0, \tag{43}$$

$$\overline{wq}\frac{\partial\overline{Q}}{\partial z} - \frac{1}{2}\frac{\partial\overline{wq^2}}{\partial z} - N_q = 0, \tag{44}$$

where the first terms represents the production of SV, the flux divergence terms again act to redistribute the variance, and N_θ and N_q are one-half the dissipation rate of potential temperature variance and specific humidity variance, respectively. These terms are made dimensionless by dividing these terms by $\kappa z/u_* x_*^2$ where $x = \theta, q$. Rearrangement of the dimensionless expressions results in the SV dissipation functions

$$\phi_{N_\theta}(\zeta) = \frac{N_\theta \kappa z}{u_* T_*^2} = \phi_h(\zeta) - \phi_{t\theta}(\zeta) \tag{45}$$

and

$$\phi_{N_q}(\zeta) = \frac{n_q \kappa z}{u_* q_*^2} = \phi_w(\zeta) - \phi_{tq}(\zeta). \tag{46}$$

The dissipation, production, and transport terms in each of these equations are expected to go as $\zeta^{-1/3}$ in the local free-convective limit (Wyngaard 1973).

The SV dissipation rates are computed using our estimates of the SV spectra in the inertial subrange. In this subrange, the Kolmogorov variance spectrum for temperature and humidity is

$$k\Phi_x(k) = \frac{fS_x(f)}{T_{xx}} = \alpha_x \epsilon^{-1/3} N_x \left(\frac{2\pi f}{\overline{U}}\right)^{-2/3}, \tag{47}$$

where α_x is the Obukhov–Corrsin constant and

$$T_{xx} = 1 - \frac{1}{9}\frac{\sigma_u^2}{(\overline{U})^2} + \frac{1}{3}\frac{(\sigma_v^2 + \sigma_w^2)}{(\overline{U})^2}, \tag{48}$$

as given by Wyngaard and Clifford (1977). The investigations provided by Hill (1989a,b) and Andreas (1987) have shown that the temperature and humidity functions are equal and must share the same value of the Obukhov–Corrsin constant within the constraints of MO similarity theory. In this investigation we have used value of $\alpha_x = 0.80$ reported by Wyngaard and Coté (1971), Paquin and Pond (1971), Champagne et al. (1977), and Högström (1996).

Our plots of the dimensionless scalar dissipation functions are shown in Fig. 9. The dotted line drawn in the

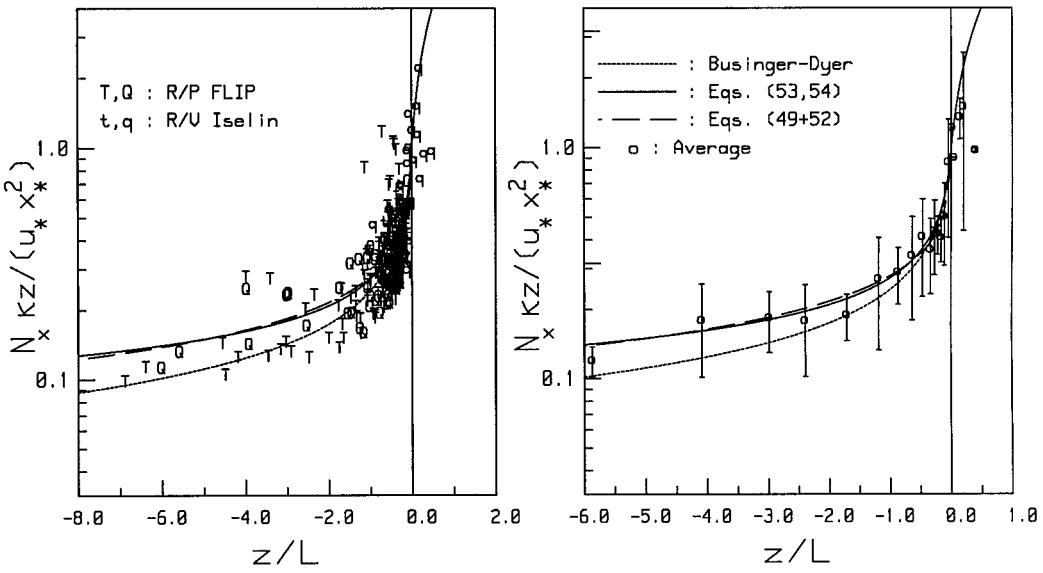

FIG. 9. Estimates of one-half the dimensionless dissipation rate of temperature variance, N_θ, and specific humidity variance, N_q, as a function of z/L. The left-hand panel displays the raw data, while the right-hand panel shows the the bin-averaged results. The error bars denote the standard error. The dotted line represents the Businger–Dyer formulation of the dimensionless scalar gradient function given by (49). The other lines drawn in the figure are identified by the equation numbers as given in the text.

figure represents the Businger–Dyer formulation for the dimensionless scalar profiles,

$$\phi_y(\zeta) = (1 - 16\zeta)^{-1/2}, \qquad \zeta < 0, \qquad (49)$$

where $y = h, w$. Although the exponent used in this function does not agree with our prediction in the convective limit, a number of field experiments (Businger et al. 1971; Dyer 1974; Dyer and Bradley 1982) have shown that it provides a better fit to the data in near-neutral conditions than a function with a $(-\zeta)^{-1/3}$ dependency. Our data also exhibit good agreement with this function in near-neutral conditions. However, the agreement between our averaged data and the Businger–Dyer formulation clearly worsens as the conditions become more convective. This suggests that the transport terms are no longer negligible in convective conditions.

We can infer something about the dimensionless form of the transport terms by using our SV flux estimates with the derivative approach explained above. In the local free convective limit we have

$$\phi_x(\zeta) = \frac{\overline{wx^2}}{u_* x_*^2} = \frac{\overline{wx^2}}{u_f x_f^2}\frac{u_f x_f^2}{u_* x_*^2} = B(-\zeta)^{-1/3}, \qquad \zeta < -1, \qquad (50)$$

where the numerical constant includes the von Kármán constant as $B = b\kappa^{1/3}$. The plot of this function is shown in Fig. 10, where the broken line in this figure is our convective limit prediction. The constant that gives the best agreement between our data and the prediction is given by $B = 1$. The averaged data in this figure follow the free-convective prediction to about $-\zeta = 0.5$ and then abruptly returns to the origin. This behavior is consistent with the results reported by Wyngaard and Coté (1971). We can parameterize this behavior with a fairly simple function shown by the solid line in this figure, which is given by

$$\phi_x(\zeta) = -18\zeta(1 - 8\zeta)^{-4/3}, \qquad \zeta < 0. \qquad (51)$$

This function provides good agreement with the data in unstable conditions and has the proper form in the free-convective limit. The function is easily differentiated to

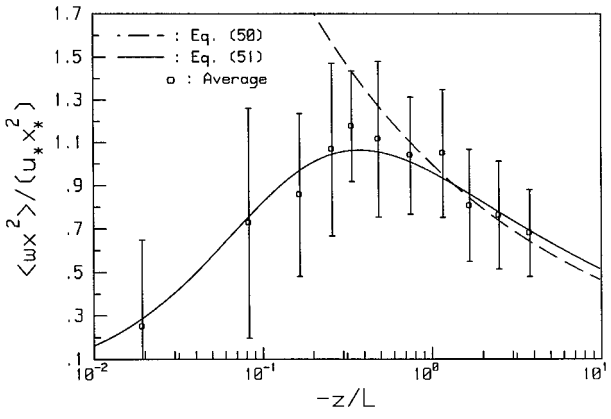

FIG. 10. Estimates of the dimensionless temperature variance flux, $\overline{w\theta^2}$, and specific humidity variance flux, $\overline{wq^2}$, as a function of z/L. The symbols denote our bin-averaged results. The error bars denote the standard error. The lines drawn in the figure are identified by the equation numbers as given in the text.

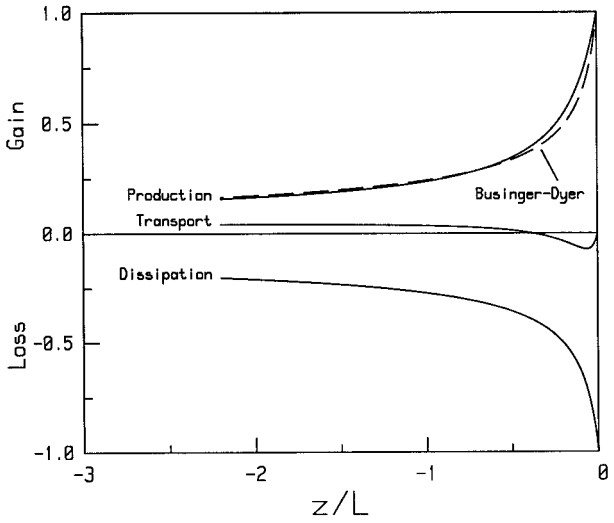

FIG. 11. The dimensionless scalar variance budget terms proposed in this paper. The turbulent transport is given by (52) and the dissipation by (53). The production term is the sum of these two functions. The broken line is the Businger–Dyer formulation for the production term.

obtain a form of the dimensionless transport function given by

$$\phi_{tx}(\zeta) = -\frac{\kappa}{6}[(24\zeta)^2(1-8\zeta)^{-7/3} - 3\phi_x(\zeta)], \qquad \zeta < 0. \tag{52}$$

The behavior of this transport term is consistent with the observations of Deardorff (1966) and Wyngaard and Coté (1971). It represents a loss of SV in near-neutral conditions and a slight gain in very unstable conditions, as shown in Fig. 11.

The dimensionless dissipation function can then be parameterized by inserting (49) and (52) in (45) and (46). The sum of these two functions agrees very well with our averaged data, as shown by the broken line in Fig. 9. Unfortunately, besides being rather cumbersome, this function does not strictly have the proper convective form. However, we can use the good agreement between the Businger–Dyer formulation and our near-neutral data to determine an estimate of the dimensionless SV dissipation function that has the correct convective limit form and is in good agreement with the measurements over the entire range of data. This function is represented by the solid line in Fig. 9 and is given by

$$\phi_{N_x}(\zeta) = (1-\zeta)^{1/6}(1-16\zeta)^{-1/2}, \qquad \zeta < 0. \tag{53}$$

The production curve in Fig. 11 represents the sum of (52) and (53).

Finally, our results have shown no clear trend in the dimensionless SV fluxes under stable conditions. This suggests that the derivative of this function (and therefore the turbulent transport) is negligible under these conditions, such that production equals dissipation. Although we have a limited amount of data in stable conditions, we obtain good agreement using the same constant that we have used for the dimensionless shear such that

$$\phi_{N_x}(\zeta) = \phi_h(\zeta) = 1 + 6\zeta, \qquad \zeta > 0. \tag{54}$$

This is consistent with the findings that the dimensionless shear and profile functions are identical under stable conditions (e.g., Panofsky and Dutton 1984).

7. The structure functions

The method used above to compute the dissipation rates of temperature and humidity variance requires us to combine TKE dissipation rates (computed from our velocity spectra) with our scalar spectra. This approach can become problematic when the instruments used to measure the velocity and scalar quantities are not collocated. Additionally, because we used inertial subrange techniques to determine the dissipation rates, our results on the TKE and SV budgets depend on the choice of Kolmogorov constants.

An approach that can be used to avoid these problems is to use the structure function parameter to investigate some of the characteristics of the turbulence. The dimensionless structure function parameters are known to obey MO similarity theory (Wyngaard et al. 1971b; Wyngaard et al. 1978; Friehe et al. 1975; Fairall et al. 1980; Edson et al. 1991). In fact, the relationship between the structure function parameters and the dissipation rates given by

$$C_x^2 = 4.0\alpha_x \epsilon^{-1/3} N_x \tag{55}$$

results in a form of the dimensionless structure function parameter given as

$$\frac{C_x^2 z^{2/3}}{x_*^2} = f_x(\zeta) = 4.0\alpha_x \kappa^{-2/3} \phi_{N_x}(\zeta)\phi_\epsilon(\zeta)^{-1/3}, \tag{56}$$

where x is now equal to u, θ, and q. Using the Kolmogorov and von Kármán constants used in this investigation and (40) and (42) for the dimensionless dissipation function, the dimensionless velocity structure function parameter becomes

$$f_u(\zeta) = 3.9\left[\frac{(1-\zeta)}{(1-7\zeta)} - \zeta\right]^{2/3}, \qquad \zeta < 0 \tag{57}$$

and

$$f_u(\zeta) = 3.9(1+5\zeta)^{2/3}, \qquad \zeta \geq 0. \tag{58}$$

The agreement between this function and our data is very similar to that shown in Fig. 6.

Our dimensionless scalar structure function parameter estimates are shown in Fig. 12. In this figure, the solid line is drawn using (56) with Eqs. (53) and (54) for $\phi_{N_x}(\zeta)$ and (40) and (42) for $\phi_\epsilon(\zeta)$. Alternatively, the limiting forms of the dimensionless dissipation functions predict that this function should be proportional

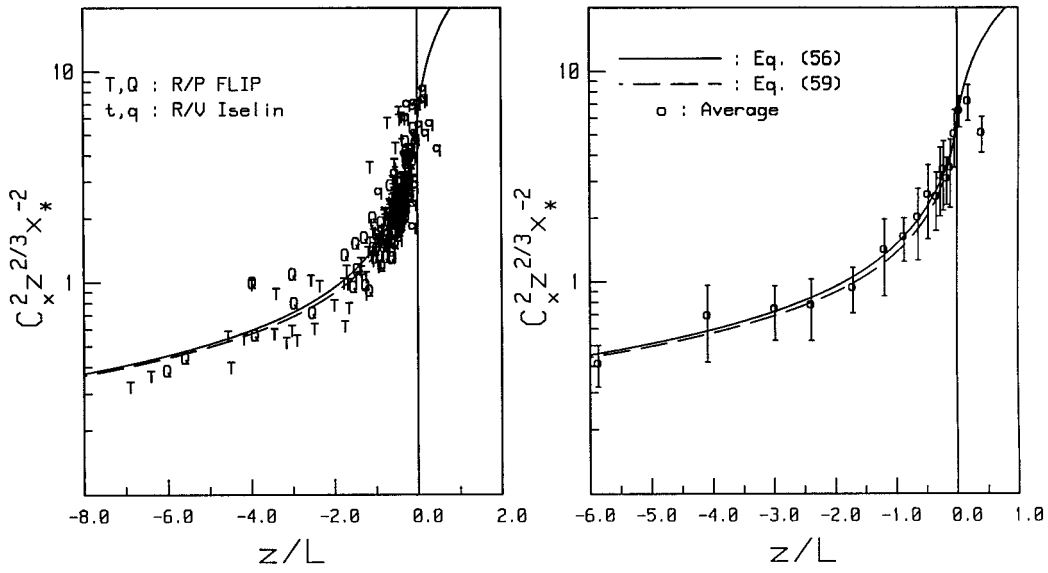

FIG. 12. Estimates of the dimensionless structure function parameter for temperature, C_θ^2, and specific humidity, C_q^2, as a function of z/L. The left-hand panel displays the raw data, while the right-hand panel shows the the bin-averaged results. The error bars denote the standard error. The lines drawn in the figure are identified by the equation numbers as given in the text.

to $-\zeta^{-2/3}$ in the convective limit. Therefore, another common approach is to use the limiting forms to simplify (56) to read

$$f_{\theta,q}(\zeta) = E(1 - F\zeta)^{-2/3}, \qquad \zeta < 0 \qquad (59)$$

in convective conditions, where E and F are another set of numerical constants. The neutral value of the dimensionless structure function parameter that agrees with both our data and our choice of the Kolmogorov and von Kármán constants is $E = 5.9$, while a value of $F = 8$ provides a good fit to our data, as shown by the broken line in Fig. 12. Our results are in close agreement with the original Kansas data (Wyngaard et al. 1971b). The closeness of these two experimental results taken more than 25 years apart with different instruments over both land and ocean is a tribute to the universality of MO similarity theory.

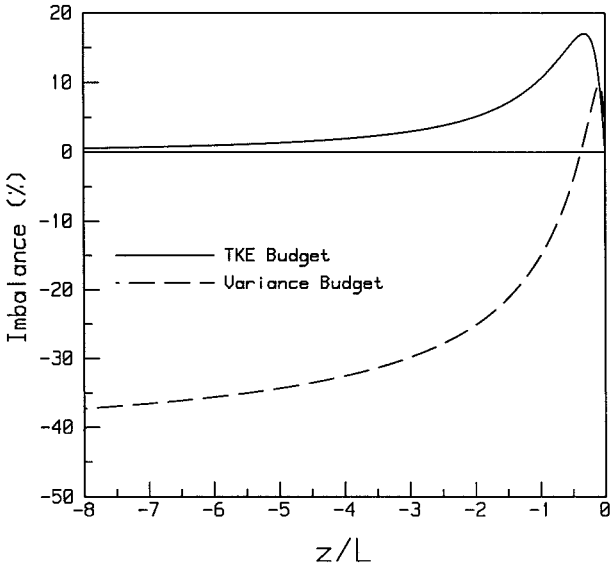

FIG. 13. The percent difference between the production and dissipation of TKE (solid line) and scalar variance (broken line) as a function of z/L. Positive values are a result of production exceeding dissipation, while negative values are a result of dissipation exceeding production.

8. Discussion

Although there is some uncertainty depending on the particular form of the dimensionless shear term, our study found that the TKE budget is well described by a balance between production and dissipation except for slightly unstable conditions where production exceeds dissipation by as much as 17% (see Fig. 13). We have argued that this is due to a local imbalance between the pressure and energy transport. Additionally, we have argued that the good agreement between our results and the overland results of Vogel and Frenzen (1992) and Frenzen and Vogel (1992) suggest that our measurements are generally taken above the WBL.

However, because the mechanisms responsible for this imbalance are still under active investigation, we recognize that part of the imbalance observed in our measurements, particularly under high wind conditions, may be due to mechanisms that do not obey MO similarity theory. For example, there have been a number of studies (e.g., Högström 1990; Wilczak et al. 1995) that have found that TKE dissipation exceeds production in near-neutral conditions. Högström (1990) concluded

that the excess of local dissipation over local production was a result of inactive turbulence (Bradshaw 1967). He argued that inactive turbulence is imported to the surface layer from the upper boundary layer through pressure transport. This extra energy is then dissipated in the surface layer, thereby creating an excess of local dissipation.

In the marine surface layer there is another plausible explanation to explain the findings of this paper, that is, that production exceeds dissipation. Over developing surface waves, part of the energy flux entering the surface layer is not dissipated into thermal energy but rather is transported to the surface to generate and sustain waves and currents. This energy flux is expected to result in a ''dissipation deficit'' in the volume-averaged dissipation rate that would result in local production exceeding dissipation. It should be noted that such a situation is not limited to the ocean; for example, a similar situation might exist over a forest canopy.

Over the ocean this deficit is expected to be a function of sea state and, as such, is not expected to obey traditional MO similarity theory. As mentioned above, preliminary results from ONR's MBL program presented by Edson et al. (1997) provides evidence for this sea state–dependent dissipation deficit. This mechanism is also consistent with the findings of Yelland and Taylor (1996), who derived an imbalance term that was a function of both stability and wind speed. Yelland and Taylor (1996) found that local production generally exceeded dissipation and that the imbalance increased with increasing wind speed.

The good agreement between our derived energy transport term and previous parameterizations suggests that some fraction of our observed dissipation deficit may be due to an additional pressure transport term that is sea state dependent. This proposition seems reasonable since the pressure flux evaluated at the surface, $\overline{wp}_0$, represents the energy flux into the waves. It might also explain differences between results taken from the open ocean (e.g., Yelland and Taylor 1996) versus coastal studies (e.g., Edson et al. 1991; Wilczak et al. 1997) due to differences in sea state at a given wind speed. For example, we expect the coastal wave field to saturate at some point due to the influence of the bottom. This would result in less energy going into the wave field as well as a rougher surface compared to the open ocean for a given wind speed. It could also explain differences between results taken from ship-based versus buoy systems due to their relative proximity to the surface.

We are now investigating these and other hypotheses using the data taken during the MBL program (e.g., Miller et al. 1997). This program is providing extensive measurements of the coupled boundary layers and wave field that allow us to compute all the terms in the KE budget. This is providing investigators with information about the sea state and has allowed us to isolate the wave-induced pressure and velocity fluctuations in the wave boundary layer (Wetzel 1996; Hare et al. 1997; Hristov et al. 1997). The main objective of this program is to improve the parameterizations provided here and to provide us with a means to extend similarity theory into the WBL.

9. Conclusions

In this paper we have examined several aspects of MO similarity theory in the surface layer over the ocean, including the various terms of the TKE budget and the SV budget equations, the Kolmogorov constant, and the dimensionless structure function parameters. These functions all have the appropriate behavior in the convective limit. In estimating these functions we opted for simple parameterizations, which seemed more appropriate because we were inferring a number of these terms through the derivative approach.

The form of the various terms in the TKE budget presented in this study closely resembled those derived from several recent overland experiments. Likewise, the form of the dimensionless SV dissipation functions and structure function parameters are in close agreement with the Kansas formulations given by Wyngaard and Coté (1971) and Wyngaard et al. (1971b). Although our measurements may be slightly influenced by wave-induced effects under high wind conditions, the good agreement between our results and previously published functions implies that MO similarity theory is valid in the marine surface layer above the WBL.

Our results agree with the theoretical requirement that the same functions be used for temperature and humidity. The parameterization for the SV transport terms were obtained using our measurements of the SV flux with the derivative approach. Our results have shown that transport terms are a slight loss of SV in near-neutral conditions and a source of SV in convective conditions, which again agrees with the Kansas observations. Our results indicate that the production of SV exceeds its dissipation by 9% in near-neutral conditions and that dissipation exceeds production by up to 13% in convective conditions as shown in Fig. 13.

In their review of the inertial–dissipation method, Fairall and Larsen (1986) noted uncertainties in the dimensionless function, the TKE, and variance budget balances, and doubts about the similarity of the temperature and moisture functions. These new results show that temperature and moisture are similar, to the accuracy of our measurements, and the uncertainties have been significantly reduced. The dimensionless structure function parameters and dissipation functions presented here are essentially complete and can be used for up-to-date applications in the inertial–dissipation flux estimation method as long as the measurements are taken above the WBL. The dimensionless structure function parameters given by (57) through (59) can be used in these algorithms without assumptions about the Kolmogorov

constants, the dimensionless gradients, or the transport functions.

Acknowledgments. This work was supported by the ONR's Remote Sensing (Grants N00014-92-J-1585 and N00014-96-1-0516) and Marine Boundary Layers (Grant N00014-93-1-0274) Programs. Support was also received from the NOAA Climate and Global Change Program and the Department of Defense Advanced Sensor Applications Program. The authors wish to thank George Young of the Pennsylvania State University and Jeffrey Hare of NOAA/ETL for their help in collecting the data and the crews of the R/V *Iselin* and the R/P *FLIP* for their outstanding efforts. We would also like to thank Reginald Hill of NOAA/ETL for his thoughtful review of this article.

REFERENCES

Anctil, F., M. A. Donelan, W. M. Drennan, and H. C. Graber, 1994: Eddy-correlation measurements of air-sea fluxes from a discus buoy. *J. Atmos. Oceanic Technol.,* **11,** 1144–1150.

Anderson, R. J., 1993: A study of wind stress and heat flux over the open ocean by the inertial-dissipation method. *J. Phys. Oceanogr.,* **23,** 2153–2161.

Andreas, E. L, 1987: On the Kolmogorov constants for the temperature–humidity cospectrum and the refractive index spectrum. *J. Atmos. Sci.,* **44,** 2399–2406.

——, 1994: Reply to ''Comment on 'Sea spray and the turbulent air–sea heat fluxes' by E. L Andreas'' by K. B. Katsaros and G. de Leeuw. *J. Geophys. Res.,* **99,** 14 345–14 350.

——, J. B. Edson, E. C. Monahan, M. P. Rouault, and S. D. Smith, 1995: The spray contribution to net evaporation from the sea. *Bound.-Layer Meteor.,* **72,** 3–52.

Banke, E. G., and S. D. Smith, 1973: Wind stress on arctic sea ice. *J. Geophys. Res.,* **78,** 7871–7883.

Bradley, E. F., P. A. Coppin, and J. S. Godfrey, 1991: Measurements of sensible and latent heat flux in the western equatorial Pacific Ocean. *J. Geophys. Res.,* **96,** 3375–3389.

Bradshaw, P., 1967: Inactive motion and pressure fluctuations in the turbulent boundary layer. *J. Fluid Mech.,* **30,** 241–258.

Businger, J. A., J. C. Wyngaard, and Y. Izumi, 1971: Flux profile relationships in the atmospheric surface layer. *J. Atmos. Sci.,* **28,** 181–189.

Carl, D. M., T. C. Tarbell, and H. A. Panofsky, 1973: Profiles of wind and temperature from towers over homogeneous terrain. *J. Atmos. Sci.,* **30,** 788–794.

Champagne, F. H., C. A. Friehe, J. C. LaRue, and J. C. Wyngaard, 1977: Flux measurements, flux estimation techniques, and fine scale turbulence measurements in the unstable surface layer over land. *J. Atmos. Sci.,* **34,** 515–530.

Deardorff, J. W., 1966: The counter-gradient heat flux in the lower atmosphere and in the laboratory. *J. Atmos. Sci.,* **23,** 503–506.

——, 1970: Convective velocity and temperature scales for the unstable planetary boundary layer and for Rayleigh convection. *J. Atmos. Sci.,* **27,** 1211–1213.

DeCosmo, J., K. B. Katsaros, S. D. Smith, R. J. Anderson, W. A. Oost, K. Bumke, and A. L. M. Grant, 1996: Air–sea exchange of sensible heat and water vapor over whitecap sea states. *J. Geophys. Res.,* **101,** 12 001–12 016.

Donelan, M. A., F. W. Dobson, S. D. Smith, and R. J. Anderson, 1993: On the dependence of sea surface roughness on wave development. *J. Phys. Oceanogr.,* **23,** 2143–2149.

Dyer, A. J., 1974: A review of flux profile relationships. *Bound.-Layer Meteor.,* **7,** 363–372.

——, and B. B. Hicks, 1970: Flux-gradient relationships in the constant flux layer. *Quart. J. Roy. Meteor. Soc.,* **96,** 715–721.

——, and E. F. Bradley, 1982: An alternative analysis of the flux-gradient relationships at the 1976 ITCE. *Bound.-Layer Meteor.,* **22,** 3–19.

——, and B. B. Hicks, 1982: Kolmogoroff constants at the 1976 ITCE. *Bound.-Layer Meteor.,* **22,** 137–150.

Edson, J. B., C. W. Fairall, S. E. Larsen, and P. G. Mestayer, 1991: A study of the inertial-dissipation technique for computing air–sea fluxes. *J. Geophys. Res.,* **96,** 10 689–10 711.

——, S. Wetzel, C. Friehe, S. Miller, and T. Hristov, 1997: Energy flux and dissipation profiles in the marine surface layer. *Proc. 12th Symp. on Boundary Layers and Turbulence,* Vancouver, BC, Canada, Amer. Meteor. Soc., 314–315.

——, A. A. Hinton, K. E. Prada, J. E. Hare, and C. W. Fairall, 1998: Direct covariance flux estimates from mobile platforms at sea. *J. Atmos. Oceanic Technol.,* **15,** 547–562.

Fairall, C. W., and S. E. Larsen, 1986: Inertial dissipation methods and turbulent fluxes at the air ocean interface. *Bound.-Layer Meteor.,* **34,** 287–301.

——, G. E. Schacher, K. L. Davidson, and T. M. Houlihan, 1980: Measurements of the humidity structure function parameters C_q^2 and C_{tq} over the ocean. *Bound.-Layer Meteor.,* **19,** 81–92.

——, E. F. Bradley, D. P. Rogers, J. B. Edson, and G. S. Young, 1996a: Bulk parameterization of air–sea fluxes for TOGA COARE. *J. Geophys. Res.,* **101,** 3747–3764.

——, ——, J. S. Godfrey, G. A. Wick, J. B. Edson, and G. S. Young, 1996b: Cool-skin and warm-layer effects on sea surface temperature. *J. Geophys. Res.,* **101,** 1295–1308.

——, A. B. White, J. B. Edson, and J. E. Hare, 1997: Integrated shipboard measurements of the marine boundary layer. *J. Atmos. Oceanic Technol.,* **14,** 338–359.

Frederickson, P., K. L. Davidson, and J. B. Edson, 1997: A study of wind stress determination methods from a ship and an offshore tower. *J. Atmos. Oceanic Technol.,* **14,** 822–834.

Frenzen, P., and C. A. Vogel, 1992: The kinetic energy budget in the surface layer: A review and an experimental reexamination in the field. *Bound.-Layer Meteor.,* **60,** 49–76.

Friehe, C. A., J. C. LaRue, F. H. Champagne, C. H. Gibson, and G. F. Dreyer, 1975: Effect of temperature and humidity fluctuations on the optical refractive index in the marine boundary layer. *J. Opt. Soc. Amer.,* **65,** 1502–1511.

Fujitani, T., 1981: Direct measurement of turbulent fluxes over the sea during AMTEX. *Pap. Meteor. Geophys.,* **32,** 119–134.

——, 1985: Method of turbulent flux measurement on a ship by using a stable platform system. *Pap. Meteor. Geophys.,* **36,** 157–170.

Garratt, J. R., 1972: Studies of turbulence in the surface layer over water (Lough Neagh). Part II: Production and dissipation of velocity and temperature fluctuations. *Quart. J. Roy. Meteor. Soc.,* **98,** 642–657.

Geernaert, G. L., K. B. Katsaros, and K. Richter, 1986: Variation of the drag coefficient and its dependence on sea state. *J. Geophys. Res.,* **91,** 4762–4779.

Godfrey, J. S., and A. C. M. Beljaars, 1991: On the turbulent fluxes of buoyancy, heat, and moisture at the air–sea interface at low wind speeds. *J. Geophys. Res.,* **96,** 22 043–22 048.

Hare, J. E., T. Hara, J. B. Edson, and J. Wilczak, 1997: A similarity analysis of the structure of air flow over surface waves, *J. Phys. Oceanogr.,* **27,** 1018–1037.

Hill, R. J., 1989a: Implication of Monin–Obukhov similarity theory for scalar quantities. *J. Atmos. Sci.,* **46,** 2236–2244.

——, 1989b: Structure functions and spectra of scalar quantities in the inertial-convective and viscous-convective ranges of turbulence. *J. Atmos. Sci.,* **46,** 2245–2251.

——, 1996: Corrections to Taylor's frozen turbulence approximation. *Atmos. Res.,* **40,** 153–175.

Högström, U., 1990: Analysis of turbulence structure in the surface layer with a modified similarity formulation for near neutral conditions. *J. Atmos. Sci,* **47,** 1949–1972.

——, 1996: Review of some basic characteristics of the atmospheric surface layer. *Bound.-Layer Meteor.,* **78,** 215–246.
Højstrup, J., 1982: Velocity spectral in the unstable planetary boundary layer. *J. Atmos. Sci.,* **39,** 2239–2248.
Hristov, T., C. Friehe, S. Miller, J. Edson, and S. Wetzel, 1997: Structure of the atmospheric surface layer over the ocean waves—Phase averaging via the Hilbert transform. *Proc. 12th Symp. on Boundary Layers and Turbulence,* Vancouver, BC, Canada, Amer. Meteor. Soc., 283–284.
Izumi, Y., 1971: Kansas 1968 field program data report. Air Force Cambridge Res. Lab. AFCRL-72-0041, Environ. Res. Paper No. 379, Hanscom AFB, MA, 79 pp. [NTIS AD 739165.]
Kaimal, J. C., J. C. Wyngaard, and D. A. Haugen, 1968: Deriving power spectra from sonic anemometers. *J. Appl. Meteor.,* **7,** 827–837.
——, ——, Y. Izumi, and O. R. Cote, 1972: Spectral characteristics of surface layer turbulence. *Quart. J. Roy. Meteor. Soc.,* **98,** 563–589.
Katsaros, K. B., and G. de Leeuw, 1994: Comment on ''Sea spray and the turbulent air-sea heat fluxes'' by E. L Andreas. *J. Geophys. Res.,* **97,** 14 339–14 343.
——, S. D. Smith, and W. A. Oost, 1987: HEXOS—Humidity Exchange Over the Sea: A program for research on water vapor and droplet fluxes from sea to air at moderate and high wind speeds. *Bull. Amer. Meteor. Soc.,* **68,** 466–476.
——, and Coauthors, 1994: Measurements of humidity and temperature in the marine environment during the HEXOS main experiment. *J. Atmos. Oceanic Technol.,* **11,** 964–981.
Keuttner, J. P., and J. Holland, 1969: The BOMEX project. *Bull. Amer. Meteor. Soc.,* **50,** 394–402.
Kolmogorov, A. N., 1941: Dissipation of energy in the locally isotropic turbulence. *Dokl. Akad. Nauk SSSR,* **32,** 16–18.
Kropfli, R. A., and S. F. Clifford, 1994: The San Clemente Ocean Probing Experiment: A study of air–sea interactions with remote and in-situ sensors. *IGARSS '94,* Pasadena, CA, IEEE, 2407–2409.
Large, W. G., and S. Pond, 1981: Open ocean momentum flux measurements in moderate to strong winds. *J. Phys. Oceanogr.,* **11,** 324–336.
——, and ——, 1982: Sensible and latent heat flux measurements over the ocean. *J. Phys. Oceanogr.,* **12,** 464–482.
Larsen, S. E., J. B. Edson, C. W. Fairall, and P. G. Mestayer, 1993: Measurement of temperature spectra by a sonic anemometer. *J. Atmos. Oceanic Technol.,* **10,** 345–354.
Liu, W. T., K. B. Katsaros, and J. A. Businger, 1979: Bulk parameterization of the air–sea exchange of heat and water vapor including the molecular constraints at the interface. *J. Atmos. Sci.,* **36,** 1722–1735.
Lumley, J. L., and H. A. Panofsky, 1964: *The Structure of Atmospheric Turbulence.* J. Wiley and Sons, 229 pp.
——, and E. A. Terray, 1983: Kinematics of turbulence convected by a random wave field. *J. Phys. Oceanogr.,* **13,** 2000–2007.
Maat, N., C. Kraan, and W. A. Oost, 1991: The roughness of wind waves. *Bound.-Layer Meteor.,* **54,** 89–103.
McBean, G. A., and J. A. Elliott, 1975: The vertical transport of kinetic energy by turbulence and pressure in the boundary layer. *J. Atmos. Sci.,* **32,** 753–766.
Miller, S., C. Friehe, T. Hristov, and J. Edson, 1997: Wind and turbulence profiles in the surface over the ocean. *Proc. 12th Symp. on Boundary Layers and Turbulence,* Vancouver, BC, Canada, Amer. Meteor. Soc., 308–309.
Monin, A. S., and A. M. Obukhov, 1954: Basic laws of turbulent mixing in the surface layer of the atmosphere. *Trudy Geofiz. Inst. Aca. Nauk SSSR,* **24,** 163–187.
Obukhov, A. M., 1946: Turbulence in an atmosphere with non-uniform temperature. *Trudy Inst. Teoret. Geofiz. Nauk SSSR,* **1,** 95–115 (translation in *Bound.-Layer Meteorol.,* **2,** 7–29, 1971).
Oost, W. A., C. W. Fairall, J. B. Edson, S. D. Smith, R. J. Anderson, J. A. B. Wills, K. B. Katsaros, and J. DeCosmo, 1994: Flow distortion calculations and their application in HEXMAX. *J. Atmos. Oceanic Technol.,* **11,** 366–386.
Panofsky, H. A., and J. A. Dutton, 1984: *Atmospheric Turbulence.* J. Wiley and Sons, 397 pp.
Paquin, J. E., and S. Pond, 1971: The determination of the Kolmogorov constants for velocity, temperature and humidity fluctuations and some second- and third-order structure functions. *J. Fluid Mech.,* **50,** 257–269.
Rieder, K. F., J. A. Smith, and R. A. Weller, 1994: Observed directional characteristics of the wind, wind stress, and surface waves on the open ocean. *J. Geophys. Res.,* **99,** 22 589–22 596.
Schmitt, K. F., C. A. Friehe, and C. H. Gibson, 1978: Humidity sensitivity of atmospheric temperature sensors by salt contamination. *J. Phys. Oceanogr.,* **8,** 141–161.
——, ——, and ——, 1979: Structure of marine surface layer turbulence. *J. Atmos. Sci.,* **36,** 602–618.
Skupniewicz, C. E., and K. L. Davidson, 1991: Hot-film measurements from a small buoy: Surface wind stress measurements using the inertial dissipation method. *J. Atmos. Oceanic Technol.,* **8,** 309–321.
Smith, S. D., 1988: Coefficients for sea surface wind stress, heat flux, and wind profiles as a function of wind speed and temperature. *J. Geophys. Res.,* **93,** 15 467–15 472.
——, and Coauthors, 1992: Sea surface wind stress and drag coefficients: The HEXOS results. *Bound.-Layer Meteor.,* **60,** 109–142.
——, C. W. Fairall, G. L. Geernaert, and L. Hasse, 1996: Air–sea fluxes: 25 years of progress. *Bound.-Layer Meteor.,* **78,** 247–290.
Stewart, R. W., 1963: Reconciliation of the available experimental data concerning the spectrum and asymmetry of locally isotropic turbulence. *Dokl. Akad. Nauk SSSR,* **152,** 324–326.
Tatarskii, V. I., 1971: *The Effects of the Turbulent Atmosphere on Wave Propagation.* Keter Press, 471 pp.
Tennekes, H., 1970: Free convection in the turbulent Ekman layer of the atmosphere. *Phys. Fluids,* **11,** 669–671.
Thiermann, V., and H. Grassl, 1992: The measurement of turbulent surface layer fluxes by use of bichromatic scintillation. *Bound.-Layer Meteor.,* **58,** 367–389.
Tsukomoto, O., E. Ohtaki, H. Ishida, M. Horiguchi, and Y. Mitsuta, 1990: On-board direct measurements of turbulent fluxes over the open sea. *J. Meteor. Soc. Japan,* **68,** 203–211.
van Atta, C. W., and W. Y. Chen, 1970: Structure functions of turbulence in the atmospheric boundary layer over the ocean. *J. Fluid Mech.,* **44,** 145–159.
Vogel, C. A., and P. Frenzen, 1992: A new study of the TKE budget in the surface layer. Part II: The dimensionless function and divergent transport terms. *Proc. 10th Symp. on Turbulence and Diffusion,* Portland, OR, Amer. Meteor. Soc., 161–164.
Webster, P. J., and R. Lukas, 1992: TOGA COARE: The coupled ocean–atmosphere response experiment. *Bull. Amer. Meteor. Soc.,* **73,** 1377–1416.
Wetzel, S. W., 1996: An investigation of wave-induced momentum flux through phase averaging of open ocean wind and wave fields. M.S. thesis, Department of Civil Engineering, Massachusetts Institute of Technology, 93 pp.
Wilczak, J., A. J. Bedard, J. Edson, J. Hare, J. Højstrup, and L. Mahrt, 1995: Pressure transport measured from a sea mast during the RASEX program. *Proc. 11th Symp. on Boundary Layers and Turbulence,* Charlotte, NC, Amer. Meteor. Soc., 489–492.
——, J. Edson, T. Hara, J. Højstrup, and J. Hare, 1997: The turbulent kinetic energy budget during RASEX. *Proc. 12th Symp. on Boundary Layers and Turbulence,* Vancouver, BC, Amer. Meteor. Soc., 312–313.
Wyngaard, J. C., 1973: On surface layer turbulence. *Workshop on Micrometeorology,* D. A. Haugen, Ed., Amer. Meteor. Soc., 101–149.
——, 1992: Atmospheric turbulence. *Annu. Rev. Fluid Mech.,* **24,** 205–233.
——, and O. R. Coté, 1971: The budgets of turbulent kinetic energy

and temperature variance in the atmospheric surface layer. *J. Atmos. Sci.,* **28,** 190–201.

——, and S. F. Clifford, 1977: Taylor's hypothesis and high frequency turbulence spectra. *J. Atmos. Sci.,* **34,** 922–929.

——, and M. A. Lemone, 1980: Behavior of the refractive index structure function in the entraining convective boundary layer. *J. Atmos. Sci.,* **37,** 1573–1585.

——, O. R. Coté, and Y. Izumi, 1971a: Local free convection, similarity, and the budgets of shear stress and heat flux. *J. Atmos. Sci.,* **28,** 1171–1182.

——, Y. Izumi, and S. A. Collins, 1971b: Behavior of the refractive-index structure function parameter near the ground. *J. Opt. Soc. Amer.,* **61,** 1646–1650.

——, W. T. Pennell, D. H. Lenschow, and M. A. Lemone, 1978: The temperature-humidity covariance budget in the convective boundary layer. *J. Atmos. Sci.,* **35,** 47–58.

Yelland, M. J., and P. K. Taylor, 1996: Wind stress measurements from the open ocean. *J. Phys. Oceanogr.,* **26,** 541–558.

——, ——, I. E. Consterdine, and M. H. Smith, 1994: The use of the inertial dissipation technique for shipboard wind stress determination. *J. Atmos. Oceanic Technol.,* **11,** 1093–1108.